Real-time label-free monitoring of adipose-derived stem cell differentiation with electric cell-substrate impedance sensing

Real-time label-free monitoring of adipose-derived stem cell differentiation with electric cell-substrate impedance sensing

Pierre O. Bagnaninchi[1] and Nicola Drummond

Medical Research Council Centre for Regenerative Medicine, University of Edinburgh, Edinburgh EH16 4SB, United Kingdom

Edited[†] by Ivar Giaever, Applied BioPhysics, Inc., Troy, NY, and approved March 11, 2011 (received for review January 12, 2011)

Real-time monitoring of stem cells (SCs) differentiation will be critical to scale-up SC technologies, while label-free techniques will be desirable to quality-control SCs without precluding their therapeutic potential. We cultured adipose-derived stem cells (ADSCs) on top of multielectrode arrays and measured variations in the complex impedance Z* throughout induction of ADSCs toward osteoblasts and adipocytes. Z* was measured up to 17 d, every 180 s, over a 62.5–64kHz frequency range with an ECIS Zθ instrument. We found that osteogenesis and adipogenesis were characterized by distinct Z* time-courses. Significant differences were found ($P = 0.007$) as soon as 12 h post induction. An increase in the barrier resistance (Rb) up to 1.7 ohm·cm^2 was associated with early osteo-induction, whereas Rb peaked at 0.63 ohm·cm^2 for adipo-induced cells before falling to zero at $t = 129$ h. Dissimilarities in Z* throughout early induction (<24 h) were essentially attributed to variations in the cell-substrate parameter α. Four days after induction, cell membrane capacitance (Cm) of osteo-induced cells (Cm = 1.72 ± 0.10 μF/cm^2) was significantly different from that of adipo-induced cells (Cm = 2.25 ± 0.27 μF/cm^2), indicating that Cm could be used as an early marker of differentiation. Finally, we demonstrated long-term monitoring and measured a shift in the complex plane in the middle frequency range (1 kHz to 8 kHz) between early ($t = 100$ h) and late induction ($t = 380$ h). This study demonstrated that the osteoblast and adipocyte lineages have distinct dielectric properties and that such differences can be used to perform real-time label-free quantitative monitoring of adult stem cell differentiation with impedance sensing.

noninvasive quantitative monitoring | bioimpedance

Several sources of stem cells are exploited and investigated for regenerative medicine, either to conduct in situ cell therapy or to facilitate drug discovery with in vitro stem cell-based disease models.

Among them, adipose-derived stem cells (ADSCs) are adult stem cells isolated at high concentration from lipoaspirates (1, 2). They are a realistic autologous source for orthopedic and reconstructive surgery applications (3) and to develop patient-specific in vitro models for drug screening.

A variety of biochemical assays are available to characterize stem cells at the molecular level. These assays have vastly contributed to improve our understanding of basic cell biology down to gene and protein expression. Paradoxically, most of these techniques are not able to characterize cells without precluding their therapeutic potential. Label-free noninvasive monitoring techniques are desirable to translate successfully basic stem cell technology to therapeutic applications. Without being able to fix, stain, lyse, or fluorescent-label the cells, few techniques remain available.

Electric cell-substrate impedance sensing (ECIS) pioneered by Giaever and Keese (4–7) is a well established technique originally developed to assess barrier formation and cell motility (8–10). The complex impedance of a cell-microelectrode interface is monitored over time through measurement of in-phase and out-of-phase signals by using a lock-in amplifier. Recent advances in the microfabrication of disposable gold electrode arrays have made the method attractive for research and commercial exploitation (Applied Biophysics, Roche Diagnostics, and MDS Analytical Technologies). This technique has found many applications in cell biology, for example, in the study of cell proliferation and spreading (11, 12), wound healing (13), cancer cell lines (14–16), and cytotoxicity (17–23). Biological cells are dielectric particles that alter the electrode impedance when interfacing with the microelectrode surface. In general, the size of the measuring electrode is several times smaller than the counter electrode to restrict the impedance measurement to the electrode–cell interface. Multifrequency complex impedance (Z^*) variations can be related to cell inherent dielectric properties, cell coverage, establishment of cell-to-cell junctions, and cell–substrate interactions. These parameters have been defined and implemented in a well-established ECIS model (6, 9) enabling a better understanding of cellular events acting on the complex impedance.

Because some cell lineages have been demonstrated to have distinct dielectric properties (24–32), and that dramatic changes occur at many levels during cell differentiation, we postulated that variations in impedance could be measured once adult stem cells were induced toward distinct lineages, enabling time-course study of cell induction.

In this study, we demonstrated real-time, label-free monitoring of adipose-derived stem cell differentiation toward osteoblasts and adipocytes with impedance sensing. Complex impedance over a 62.5- to 64-kHz frequency range was monitored for >2 wk after cell induction with an Electric Cell-Substrate Impedance Sensing system (ECIS Zθ; Applied Biophysics). Complex impedance measurements, dielectric properties, intercellular junctions, cell–substrate interactions, and complex plane anaysis were undertaken to elucidate differences in the observed bioimpedance throughout differentiation.

Results

Osteogenesis and Adipogenesis Are Characterized by Distinct Impedance Time-Courses. Fig. 1*A* shows the magnitude of the time and frequency-dependent impedance $|Z(t,f)|$ at $f = 64$ kHz over 200 h for four groups ($n = 3$): no cell control, noninduced, osteo-induced, and adipo-induced. Data were collected in two eight-well plates containing 40 gold microelectrodes per wells. Different trends in $|Z(t,64\ \text{kHz})|$ were clearly identifiable after induction ($t = 93$ h). Impedance of noninduced cells leveled off at confluency and drop to no-cell control value when spontaneous detachment occurred after media was changed ($t = 160$ h). Osteogenesis and adipogenesis were respectively characterized

Author contributions: P.O.B. designed research; P.O.B. and N.D. performed research; P.O.B. analyzed data; and P.O.B. wrote the paper.

The authors declare no conflict of interest.

[†]This Direct Submission article had a prearranged editor.

Freely available online through the PNAS open access option.

[1]To whom correspondence should be addressed. E-mail: pierre.bagnaninchi@ed.ac.uk.

This article contains supporting information online at www.pnas.org/lookup/suppl/doi:10.1073/pnas.1018260108/-/DCSupplemental.

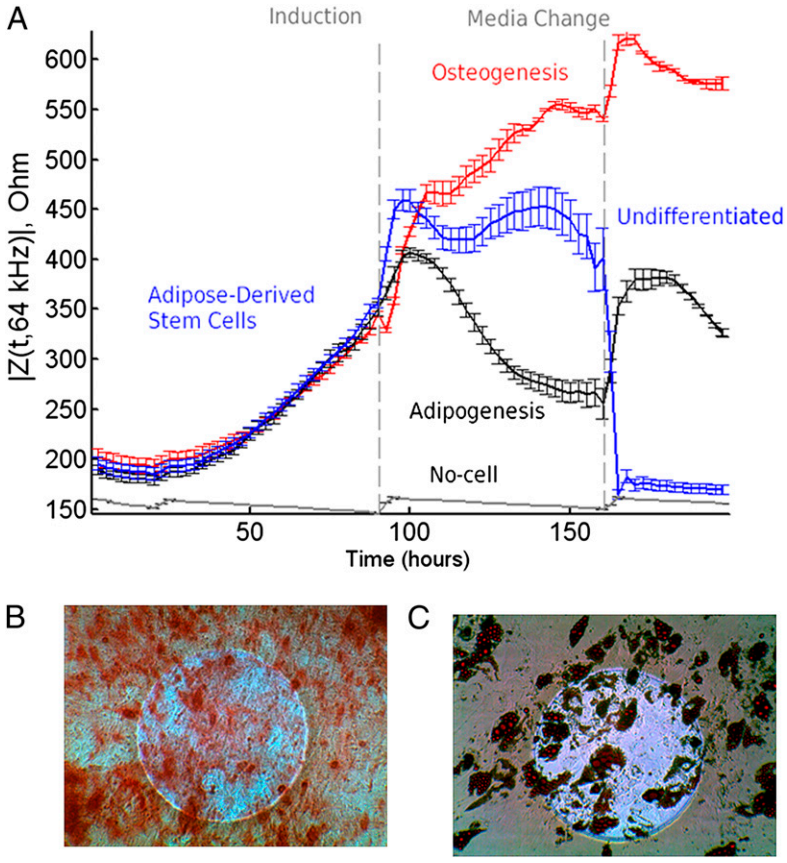

Fig. 1. Real-time and label-free monitoring of ADSCs induced toward osteoblasts and adipocytes. (*A*) Time-course measurement of mean impedance, |Z(*t*,*f*)|, at 64 kHz, for different groups throughout early induction. ADSCs were seeded (t = 0) on multiwell preprinted electrodes arrays. At t = 93 h, ADSCs were induced toward osteoblasts (n = 3) and adipocytes (n = 3) with, respectively, osteogenesis and adipogenesis differentiation medium. Noninduced ADSCs (n = 3) were kept growing after confluency until cell detachment occurred. Clear differences in |Z(*t*,*f*)| can be observed between all groups. After several days (>14) after induction, histochemical end-point staining was performed to assess that cells underwent osteogenesis (*B*) (Alizarin red stain) and adipogenesis (*C*) (Oil Red O stain). Circular microelectrodes were 250 μm in diameter and appeared as bright circle on the micrograph.

by a steady increase and a gradual fall in |Z(*t*,64 kHz)|. A change of media was characterized by a peak in impedance due partly to a change in pH, temperature, and dissolved CO_2 (as observed in no cell control) but mainly to the ensuing cell response. End point staining (t > 14 d after induction) was performed to demonstrate that ADSCs were induced toward osteoblasts (Alizarin Red staining; Fig. 1*B*) or adipocytes (Oil Red O staining; Fig. 1*C*). These data indicated that osteogenesis and adipogenesis of ADSCs were characterized by distinct impedance time-course.

Early Discrimination of Osteogenesis and Adipogenesis. A map of the time- and frequency-dependent P values, obtained from a one-way ANOVA and presented in Fig. S1*A*), revealed that the impedance of osteo-induced cells was significantly higher than that of the adipo-induced cells (P = 0.007) as soon as 12 h post induction in a 4- to 16-kHz frequency interval. However, the highest frequency (64 kHz) was found to optimize the distance of normalized means between osteo-induced and adipo-induced curves from t = 135 h and thereafter (Fig. S1*B*). At this frequency, significant differences were found (P = 0.006 at t = 115 h) 22 h post induction, and afterward (Fig. S1*A*) between osteo-induced and adipo-induced groups. From t = 121 h, impedance of adipo-induced were also significantly different (P = 0.001) from non-induced group (Fig. S1*C*).

Micrographs were taken for noninduced control, osteo-induced, and adipo-induced groups 1, 2, and 4 d post induction. Phase-contrast imaging did not show obvious changes in morphology at day 1 post induction. Representative micrographs can be found on Fig. S2. In general, induced cells covered entirely the surface of the microelectrodes. At day 2, osteo-induced cells underwent a decrease in size and a tightening of cell-to-cell junctions, whereas adipo-induced cells were characterized by a slight increase in size and a loosening of intercellular junctions in good agreement with literature (2). Media was changed at day 4 post induction, and a spontaneous detachment of confluent ADSCs was observed leaving the electrode free of cells. This event corresponds to the drop in impedance to the no cell control value seen in Fig. 1*A*.

The frequency-dependent real (resistance, R) and imaginary part (capacitive reactance, Xc) of the complex impedance are plotted in Fig. 2 *A* and *B* for osteo-induced and adipo-induced ADSCs cultured on single-electrode plates. At the media change, postinduction cells were measured (n = 3) in their respective induction medium and in a common medium (DMEM supplemented with 10% FCS). No statistical differences were found between measurements taken in their respective differentiation medium and in the common medium for the osteo-induced or the adipo-induced group. As described above, clear differences were observed between the two groups whatever the medium was. These data showed that the differences in complex impedance between osteogenesis and adipogenesis were not due to the measurements being performed in different induction media, but to a difference established by the cells undergoing distinct differentiation processes. The statistical differences exposed above and these data demonstrated the ability to monitor label-free and in real-time early induction (i.e., <24 h) of ADSCs in osteoblasts and adipocytes with impedance sensing before the apparition of obvious morphological changes.

Elucidating Variation of Impedance Throughout Early Induction. Next, we applied a model developed by Giaever and Keese (6, 9) for cells covering entirely the electrodes to interpret the time-course changes observed in |Z(*t*,*f*)| during early induction. The model is based on the current pathway analysis as briefly described in *Materials and Methods*. We retrieved the barrier resistance, Rb, of the cell layer and the cell-to-substrate interaction parameter, α^2, for the adipo- and osteo-induced groups. Rb increases with

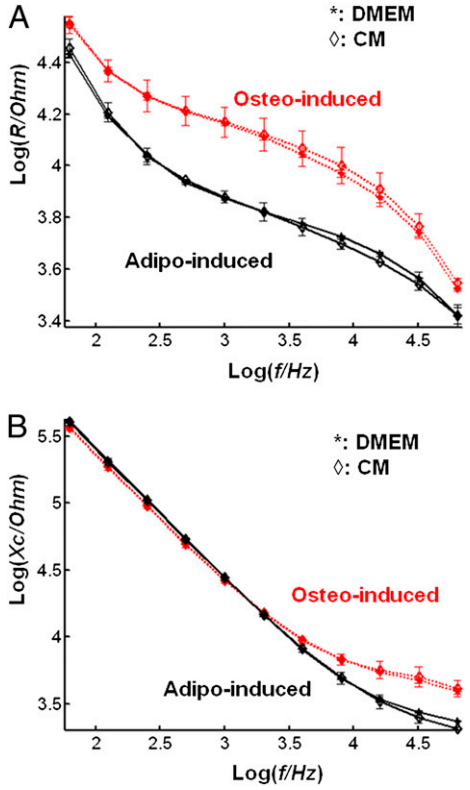

Fig. 2. Frequency-dependent resistance and capacitive reactance of osteo-induced and adipo-induced cells in different culture medium. The logarithm of the resistance, R (*A*), and of the capacitive reactance, Xc (*B*), were plotted against the logarithm of the frequency for the osteo-induced and adipo-induced groups. No significant differences were found when their respective differentiation complete medium (CM) was switched for 10% FCS supplemented DMEM (DMEM). Differences observed between the two groups did not arise from differences in the differentiation media.

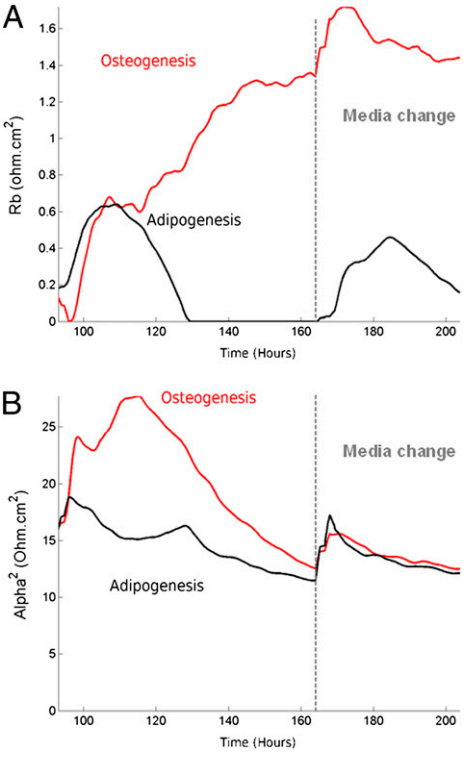

Fig. 3. Elucidating variation in impedance throughout early induction. (*A*) During osteogenesis, the barrier resistance, Rb, was found to increase steadily after induction (t = 96 h) to 1.7 ohm·cm^2 and leveled off at 1.4 ohm·cm^2 after the media was changed (t = 164 h). Rb declined after the first day of adipogenesis to reach zero at t = 129 h. The change of media was characterized by a re-establishment of the cell-to-cell junction over the next 48 h. (*B*) α^2, the cell-to substrate parameter, rose over the first day of osteo-induction to 22.5 ohm·cm^2 before falling to a mean value of 14 ohm·cm^2. α^2 decreased slowly after induction for the adipo-induction group.

the tightening of the intercellular junctions, whereas α^2 is linearly related to the mean cell surface area and, inversely, to the distance cell substrate. Briefly, Rb increased steadily up to 1.7 ohm·cm^2 during early osteogenesis, and decreased to zero at t = 129 h for adipo-induced cells (Fig. 3*A*). α^2 rose over the first day of osteo-induction to 27.7 ohm·cm^2 before falling to a mean value of 12.6 ohm·cm^2 4 d after induction (Fig. 3*B*). Adipo induction was characterized by a slight decrease in α^2 from 18.8 to 12.2 ohm·cm^2.

The parameters indicated that 24 h after induction, the differences between the impedance of the osteo- and adipo-induced groups can be mainly attributed to the establishment of intercellular junctions. During early induction (<24 h), the difference is due principally to a difference in the parameter α^2. Because no increase in size was observed for the osteo-induced group at day 1, the increase in α^2 can be attributed to a better cell-to-substrate interaction (i.e., a decrease in the cell–substrate distance, h). The subsequent fall in α^2 could be attributed to the observed decrease in cell size. Similarly, because the cell size of the adipo-induced ADSCs increased, adipogenesis was characterized by a decrease in cell-to-substrate interactions.

Cell Membrane Capacitance Is a Marker of Differentiation. We investigated the change in the mean cell membrane capacitance of differentiating cells by using single-electrode ECIS arrays. Four days after induction, mean cell membrane capacitance of cells undergoing adipogenesis (n = 6) (Cm = 2.25 ± 0.27 μF/cm^2) was significantly higher (P = 0.0008) than that of osteo-induced cells (n = 6) (Cm = 1.72 ± 0.10 μF/cm^2) as represented in Fig. S3. Moreover, adipo-induced cells were significantly different from undifferentiated ADSCs (n = 6) (Cm = 1.65 ± 0.07 μF/cm^2) 4, 7, and 15 d post induction. Cm of osteoblasts decreased significantly along differentiation (P = 0.0024) to reach a value of 1.43 ± 0.08 μF/cm^2 15 d after induction. Phase-contrast imaging (as shown in Fig. S4) confirmed that cells were confluent on the microelectrodes, as required for meaningful modeling, and that lipid droplets production occurred only 7 d after induction suggesting strongly that changes in cell membrane capacitance could be used as an early marker of differentiation.

These data showed a transition of dielectric properties throughout early induction as recently observed by dielectrophoresis (24) for mouse neural stem/precursor cells (NSPCs) differentiating into neurons and astrocytes. Taken together, Rb, α^2, and Cm indicated that the different trends in impedance observed in Fig. 1*A* translated fundamental differences in the mechanisms of osteo- and adipo-induction, and that distinct dielectric properties characterize the osteoblast and adipocyte lineages.

Long-Term Monitoring of ADSCs Differentiation. Finally, we demonstrated long-term monitoring over a 17-d period (Fig. 4*A*). The time-course of impedance at 64 kHz averaged over three wells was clearly different throughout osteogenesis and adipogenesis.

Complex plane analyses were undertaken at early (t = 100 h; Fig. 4*B*) and late differentiation (t = 380 h; Fig. 4*C*). We plotted the imaginary part against the real part of the complex impedance on a log scale at each frequency from 250 Hz to 64 kHz. The frequency is doubled at each point. These plots demon-

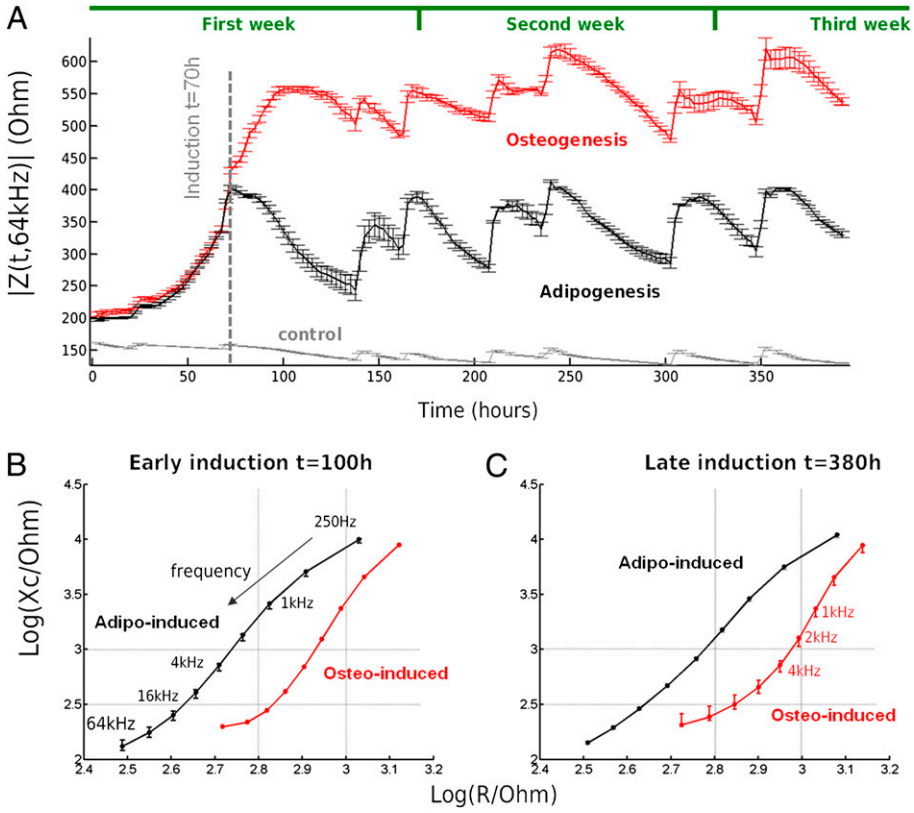

Fig. 4. Long-term monitoring of osteogenesis and adipogenesis with electric cell-substrate impedance sensing. (*A*) Long-term monitoring of |Z(*t*,*f*)| was demonstrated throughout differentiation ($t > 400$ h) and plotted at 64 kHz. At $t = 70$ h, ADSCs were induced toward osteoblasts ($n = 3$) and adipocytes ($n = 3$). (*B*) Mean complex impedance ($Z = R + iXc$) and SD represented at multiple frequencies (250 Hz to 64 kHz) in the complex plane on a logarithmic scale. Differences in the complex spectra were observed between osteo-induced and adipo-induced cells at early ($t = 100$ h) (*B*) and late (*C*) stage ($t = 380$ h) of differentiation. A shift in the complex plane can be observed between cells at early and late differentiation stage, indicating a possible correlation in the middle frequency range with the apparition of specialized functions.

strated multifrequency differences on a log scale between early and late differentiation for both osteo-induced and adipo-induced ADSCs (Fig. 4 *B* and *C*). Late induction was characterized principally on the log-scale by variations in the 1- to 8-kHz frequency range compared with early induction. Microscopically, the samples were characterized by the apparition of specialized functions, namely the production of a mineralized matrix for osteo-induced cells and formation of lipid droplets from adipocytes (Fig. 1 *B* and *C* and Fig. S4). These data indicated a possible correlation between the apparition of specialized functions and a shift of the complex impedance in the 1- to 8-kHz frequency range.

Discussion

In this study, ADSCs were used as a biological model of adult stem cell differentiation to demonstrate that different cell lineages have distinct dielectric properties, which can be exploited to monitor differentiation in real-time and label-free with impedance sensing. To increase experiment repeatability, we used commercially available differentiation medium and cell source. This work is translatable directly to mesenchymal stem cells and other sources of stem cells that can be expanded and differentiated in adherent monolayers. However, further studies will be required to validate and adapt the method to monitor embryonic stem cells and induced pluripotent stem cell differentiation. The protocols for the induction of ADSCs into osteoblastic and adipogeneic lineages are well established and resulted in morphologically and functionally distinct cell lines as described in published studies (2, 33–35). Several batches of ADSCs, and several commercially available differentiation medium (Invitrogen and R&D Systems) were tested with similar results.

We have shown that throughout differentiation differences between the impedance of osteo-induced and adipo-induced cells were well-defined at multiple frequencies. As soon as 12 h post induction, significant differences were found between the impedance of the induced groups, whereas no clear morphological differences could be found. Immunochemistry of specific markers, such as osteocalcin for osteoblasts, is generally performed 4 d after induction to get a positive staining. Similarly genome-wide analysis of genes up-regulated during osteogenesis and adipogenesis demonstrated the apparition of specific markers 2 d after induction (36). This study underlines the potential of impedance sensing in identifying and elucidating time-course events.

Throughout differentiation, a gradual reorganization of the cell layer occurred. For modeling purposes, cells were assumed to be confluent at any time-point as unsynchronized individual cellular events (cell division, morphological changes) were averaged down by the 40 electrodes. The frequency-dependent complex impedance, $Z(t,f)$, was broken down in three parameters with the model developed by Giaever and Keese (6, 9). α was found involved in early differentiation. When a confluent monolayer of a cell line such as Madin-Darby canine kidney cell (MDCK) is studied with impedance sensing (9), α can be directly linked to cell–substrate interaction. However, during stem cell differentiation, both the cell size and the distance cell substrate can vary, making its interpretation more difficult. With the additional information from microscopy, we were able to interpret distinct trends in α along osteogenesis and adipogenesis. Typical reported values (10) for α are 18 $\Omega^{1/2}$.cm ($\alpha^2 = 324\ \Omega.cm^2$) for

MDCK cells and 7 $\Omega^{1/2}$.cm (α^2 = 49 $\Omega.cm^2$) for lung fibroblastic cells WI38 VA13 cells. For an homogeneous cell layer, cell-to-substrate distance could be computed directly from α and cell radius or cell width (fibroblastic cells) (37).

Rb was found particularly involved in osteogenesis and showed that osteo-induced cells establish intercellular junctions over the course of 48 h after induction as opposed to adipogenesis. Typical values for MDCK cells can be up to 60 $\Omega.cm^2$ once they have established a barrier function and 2.2 $\Omega.cm^2$ for lung fibroblastic cells. No Rb values for osteoblasts were found in the literature; however, a transepithelial resistance (TER) of 8 $\Omega.cm^2$ is reported (38) for osteoblast-like MC3T3 cells, which can be compared with TER values of 136 $\Omega.cm^2$ for MDCK cells and 23 $\Omega.cm^2$ for WI38 VA13 cells. Note that TER values are always found larger than Rb (10). Finally, we analyzed the cell membrane capacitance, Cm, as retrieved with the ECIS model. This parameter is of particular importance for stem cell applications where one needs to assess cell identify. Indeed, dielectric properties (24–32) have been shown to discriminate different cell lines with dielectrophoresis and impedance spectroscopy. Impedance sensing measures the average Cm over all of the cells present on the electrodes, and the main limitation is that cells have to be confluent on the electrode. For that reason, we conducted a separate set of experiments on single-electrode plates where the confluence of the cell could be assessed directly microscopically before taking multifrequency measurements. After 4 d, Cm was found different between osteo- and adipo-induced cells. After 15 d, Cm reached a value of 1.43 ± 0.08 $\mu F/cm^2$ for cells induced toward osteoblasts and of 2.12 ± 0.16 $\mu F/cm^2$ for cells induced toward adipocytes. Typical cell membrane capacitance values are in the 1 $\mu F/cm^2$ range and, even though the structure of the phospholipid bilayer is similar for all cell lines, membrane folding and numbers of transmembrane proteins are found responsible for differences between cell lines or physiological states. In this study, the osteoblast and adipocyte lineages were characterized by distinct dielectric properties. Cell dielectric properties could be modeled from the impedance spectrum in different ways with basal, apical, and lateral cell membrane capacitance (9), equivalent circuit model (39), or through a mean field model (40). These models yield different values of Cm yet in the similar order of magnitude, underlining the difficulty if not the impossibility to compare values of Cm in the literature. However, these models should be explored in depth for stem cell monitoring where a bioelectrical signature could be established based on complex cellular dielectric properties. Ideally, a double shell model should be considered, which takes into account the dielectric properties of the nucleus, the cytoplasm, and the cytoplasmic membrane (41). Studies of dielectric properties of stem cells are sparse and the comparison of our results of the cell membrane capacitance is uneasy at this stage. A transition of the crossover frequency during differentiation of neural stem/progenitor cell has been demonstrated with DEP (24), although without reporting the corresponding cell membrane capacitance. A similar transition of dielectric properties throughout differentiation was demonstrated in this study. In the same study, dielectric properties of NSPCs in suspension have been found to discriminate stem cell progeny before the apparition of specific cell surface proteins (24). Impedance sensing was able to characterize cells in their physiological state as opposed to impedance spectroscopy and dielectrophoresis where measurements rely on the use of a low conductive medium that hinder time-course studies.

Finally, we have demonstrated the ability of long-term monitoring, which will be critical for stem cell differentiation studies. Typically, full differentiation in osteoblasts and adipocytes require at least 2 wk of cell culture. We demonstrated real-time monitoring over a period of 420 h (17.5 d); at this stage, cells were stained positive for alizarin red when induced toward osteoblasts and positive for Oil Red O when induced toward adipocytes. Throughout differentiation, differences between the impedance of osteo-induced and adipo-induced cells were well-defined at multiple frequencies, demonstrating the robustness of the method to monitor differentiation. Analyses in the complex plane showed a shift in the complex impedance at middle frequency (1–8 kHz) between early and late osteo-induced cells and, in a lesser amount, for adipo-induced cells, suggesting a potential correlation to the apparition of specialized functions. Additional studies comparing directly the amount of mineralized matrix and lipid droplets production to the variation of $|Z(t,f)|$ will be necessary and might require an extended frequency range not available in our current setup. Indeed, a clear contribution of inclusions containing sparse moving ions such as lipid droplets should be expected in the 1–10 MHz range (42). Nevertheless, this study demonstrated that the two lineages derived from the same cell source acquire distinct dielectric properties throughout late differentiation and establish clearly impedance sensing as a method for quantitative real-time monitoring of ADSCs differentiation toward osteoblasts and adipocytes.

Conclusion

This study demonstrated that differences in cell lineage dielectric properties can be exploited to monitor in real-time and label-free adult stem cell differentiation with impedance sensing. This technique could be translated directly to adult stem cells from other tissues, and with some key modifications to other types of stem cells. Methods for quantitative monitoring of adult stem cell differentiation could contribute to the automation of stem cell culture, the optimization and design of defined media and substrates, and to drug discovery through the screening of adult stem cell-based in vitro models.

Materials and Methods

Impedance Sensing. We used a commercial Electric Cell-Substrate Impedance Sensing system (ECIS Zθ; Applied Biophysics) to monitor time and frequency dependent complex impedance, $Z(t,f)$, of the electrode-cell interface. Resistance, R(t,f), and capacitive reactance, Xc(t,f), are respectively the real and imaginary part of Z such as $Z(t,f) = R(t,f) + iXc(t,f)$ and $|Z(t,f)|^2 = R(t,f)^2 + Xc(t,f)^2$. Cells were grown on eight-well ECIS arrays (8W1E or 8W10+; Applied Biophysics) containing one or 40 250-μm gold microelectrodes per well. Two ECIS arrays were recorded in parallel, for a total of 16 wells per experiment. Measurements were performed directly in the cell culture medium, allowing real-time monitoring, whereas both the ECIS arrays and the measurement station were kept in an incubator with high humidity at 37 °C and 5% CO_2. Multifrequency measurements (11 frequencies at 0.0625, 0.125, 0.25, 0.5, 1, 2, 4, 8, 16, 32, and 64 kHz) were taken for each of the 16 wells at a fixed 180-s interval.

Cell Culture and Induction. Human Adipose-Derived Stem Cells (ADSCs) were obtained from Invitrogen. ADSCs were cultured in complete Mesenpro RS medium (Invitrogen) with 2 mM L-glutamine according to the supplier protocol and used at passage 2. ECIS arrays were incubated with cell culture medium 2 h before cell inoculation to condition the gold film electrodes. Each well was seeded with 200 μL of cell suspension for a resulting cell density of 10,000 cells per cm^2. After cell attachment (>4 h), 200 μL of medium was added per well. At the time of induction, the medium was switched either to an osteogenesis or to an adipogenesis differentiation medium (Invitrogen). Noninduced controls were kept in complete Mesenpro RS media. When the media had to be changed every 2–3 d, the ECIS system was paused and the arrays unplugged. After the cell culture media was replaced under a biosafety cabinet class II, the arrays were then plugged back to the system and the acquisition was resumed.

Staining. End point staining (t > 14 d) was performed to demonstrate that ADSCs have been induced toward osteoblasts or adipocytes. Cells were rinsed with PBS, fixed with 3.7% formaldehyde for 20 min, and stored in PBS. ADSCs induced toward osteoblasts were stained with a solution of alizarin red for 30 min and washed several times in deionized water. A 1% solution of Oil Red O (ORO) in propan-2-ol was used to stain the lipid droplets, which were used as a marker of adipocyte differentiation. Wells were washed three times in PBS after 30 min of ORO incubation. Noninduced ADSCs were used as negative controls for both staining procedures.

ECIS Model. For this study, we used the model developed by Giaever and Keese (6), which is directly implemented in the ECIS Zθ software. When cells are confluent on the electrodes, a prerequisite for meaningful modeling, three different current pathways can be identified (6, 9) from which a model breaks down $Z(t,f)$ in three time-course frequency-independent parameters: (*i*) Rb (ohm·cm^2), a barrier resistance due to the establishment of tight cell-to-cell junctions; (*ii*) α^2(ohm·cm^2), a parameter related to cell-to-substrate interaction and linked to the mean cell radius (r) and mean cell-substrate distance (h) through the equation $\alpha^2 = r^2 \times \rho/h$, where ρ is the resisitivity of the medium; (*iii*) Cm (μF/cm^2), the average cell membrane capacitance. The reference well was set to a no-cell control with either complete Mesenpro RS medium or a osteogenic or adipogenic medium according to which group was modeled. Single-electrode (8W1E) arrays were found to retrieve Cm more accurately, and we conducted differentiation of ADSC on single-electrode arrays for this specific purpose. Data were collected on specific days because the number of arrays prevented real-time monitoring of differentiation.

Data Interpretation. Impedance data from the ECIS instrument were exported to Matlab (Mathworks) to be analyzed. For each group (no-cell control, noninduced ADSCs, osteo-induced, and adipo-induced), the mean value and SD were calculated at each time and frequency. As a result, group data were smoothed compared with raw individual data. For the sake of visibility error bars were plotted every 50 points. Mean distance of normalized values of $|Z(t,f)|$ between osteo-induced and adipo-induced group were plotted at each frequency and time. Complex plane representation of Z at selected time points were produced by plotting the real part of the complex impedance (the resistance, R in ohms) against the imaginary part, (the complex reactance, Xc, in ohms) on a log-scale between 250 Hz and 64 kHz.

Statistics. One-way ANOVA tests were performed to determine whether one group was significantly different from the others, followed by a Tukey–Kramer multicomparison test to determine which groups were significantly different. A probability level of $P < 0.01$ was set as significant. P values were plotted against time and frequency and displayed on a colormap with the saturation level set to 0.01. Areas where no significant differences were found between the groups were displayed in black on the map.

ACKNOWLEDGMENTS. P.O.B. acknowledges support from the Research Councils UK (RCUK) for his RCUK Fellowship and funding from Engineering and Physical Sciences Research Council Grant EP/G030871/1.

1. Zuk PA, et al. (2001) Multilineage cells from human adipose tissue: Implications for cell-based therapies. *Tissue Eng* 7:211–228.
2. Zuk PA, et al. (2002) Human adipose tissue is a source of multipotent stem cells. *Mol Biol Cell* 13:4279–4295.
3. Zuk PA (2010) The adipose-derived stem cell: Looking back and looking ahead. *Mol Biol Cell* 21:1783–1787.
4. Giaever I, Keese CR (1984) Monitoring fibroblast behavior in tissue culture with an applied electric field. *Proc Natl Acad Sci USA* 81:3761–3764.
5. Giaever I, Keese CR (1986) Use of electric fields to monitor the dynamical aspect of cell behavior in tissue culture. *IEEE Trans Biomed Eng* 33:242–247.
6. Giaever I, Keese CR (1991) Micromotion of mammalian cells measured electrically. *Proc Natl Acad Sci USA* 88:7896–7900.
7. Giaever I, Keese CR (1993) A morphological biosensor for mammalian cells. *Nature* 366:591–592.
8. Lo CM, Keese CR, Giaever I (1993) Monitoring motion of confluent cells in tissue culture. *Exp Cell Res* 204:102–109.
9. Lo CM, Keese CR, Giaever I (1995) Impedance analysis of MDCK cells measured by electric cell-substrate impedance sensing. *Biophys J* 69:2800–2807.
10. Lo CM, Keese CR, Giaever I (1999) Cell-substrate contact: Another factor may influence transepithelial electrical resistance of cell layers cultured on permeable filters. *Exp Cell Res* 250:576–580.
11. Mitra P, Keese CR, Giaever I (1991) Electric measurements can be used to monitor the attachment and spreading of cells in tissue culture. *Biotechniques* 11:504–510.
12. Wegener J, Keese CR, Giaever I (2000) Electric cell-substrate impedance sensing (ECIS) as a noninvasive means to monitor the kinetics of cell spreading to artificial surfaces. *Exp Cell Res* 259:158–166.
13. Keese CR, Wegener J, Walker SR, Giaever I (2004) Electrical wound-healing assay for cells in vitro. *Proc Natl Acad Sci USA* 101:1554–1559.
14. Keese CR, Bhawe K, Wegener J, Giaever I (2002) Real-time impedance assay to follow the invasive activities of metastatic cells in culture. *Biotechniques* 33:842–844, 846, 848–850.
15. Tarantola M, et al. (2010) Dynamics of human cancer cell lines monitored by electrical and acoustic fluctuation analysis. *Integr Biol (Camb)* 2:139–150.
16. Lovelady DC, Richmond TC, Maggi AN, Lo CM, Rabson DA (2007) Distinguishing cancerous from noncancerous cells through analysis of electrical noise. *Phys Rev E Stat Nonlin Soft Matter Phys* 76:041908.
17. Tarantola M, et al. (2009) Cytotoxicity of metal and semiconductor nanoparticles indicated by cellular micromotility. *ACS Nano* 3:213–222.
18. Lovelady DC, Friedman J, Patel S, Rabson DA, Lo CM (2009) Detecting effects of low levels of cytochalasin B in 3T3 fibroblast cultures by analysis of electrical noise obtained from cellular micromotion. *Biosens Bioelectron* 24:2250–2254.
19. Xiao C, Lachance B, Sunahara G, Luong JH (2002) Assessment of cytotoxicity using electric cell-substrate impedance sensing: Concentration and time response function approach. *Anal Chem* 74:5748–5753.
20. Xiao C, Luong JHT (2003) On-line monitoring of cell growth and cytotoxicity using electric cell-substrate impedance sensing (ECIS). *Biotechnol Prog* 19:1000–1005.
21. Xiao C, Luong JHT (2005) Assessment of cytotoxicity by emerging impedance spectroscopy. *Toxicol Appl Pharmacol* 206:102–112.
22. Opp D, et al. (2009) Use of electric cell-substrate impedance sensing to assess in vitro cytotoxicity. *Biosens Bioelectron* 24:2625–2629.
23. Male KB, Lachance B, Hrapovic S, Sunahara G, Luong JHT (2008) Assessment of cytotoxicity of quantum dots and gold nanoparticles using cell-based impedance spectroscopy. *Anal Chem* 80:5487–5493.
24. Flanagan LA, et al. (2008) Unique dielectric properties distinguish stem cells and their differentiated progeny. *Stem Cells* 26:656–665.
25. Pethig R, Menachery A, Pells S, De Sousa P (2010) Dielectrophoresis: A review of applications for stem cell research. *J Biomed Biotechnol* 2010:182581.
26. Stephens M, Talary MS, Pethig R, Burnett AK, Mills KI (1996) The dielectrophoresis enrichment of CD34+ cells from peripheral blood stem cell harvests. *Bone Marrow Transplant* 18:777–782.
27. Vykoukal J, Vykoukal DM, Freyberg S, Alt EU, Gascoyne PRC (2008) Enrichment of putative stem cells from adipose tissue using dielectrophoretic field-flow fractionation. *Lab Chip* 8:1386–1393.
28. Holmes D, et al. (2009) Leukocyte analysis and differentiation using high speed microfluidic single cell impedance cytometry. *Lab Chip* 9:2881–2889.
29. Cheung K, Gawad S, Renaud P (2005) Impedance spectroscopy flow cytometry: On-chip label-free cell differentiation. *Cytometry A* 65:124–132.
30. Ayliffe HE, Frazier AB, Rabbitt RD (1999) Electric impedance spectroscopy using microchannels with integrated metal electrodes. *J Microelectromech Syst* 8:50–57.
31. Bagnaninchi PO, Dikeakos M, Veres T, Tabrizian M (2004) Complex permittivity measurement as a new noninvasive tool for monitoring in vitro tissue engineering and cell signature through the detection of cell proliferation, differentiation, and pretissue formation. *IEEE Trans Nanobioscience* 3:243–250.
32. Mills KI, Stephens M, Talary M, Pethig R, Burnett AK (1995) Dielectrophoretic separation of CD34-positive cells from peripheral stem cell harvests. *Blood* 86:462.
33. Liu TM, et al. (2007) Identification of common pathways mediating differentiation of bone marrow- and adipose tissue-derived human mesenchymal stem cells into three mesenchymal lineages. *Stem Cells* 25:750–760.
34. Elabd C, et al. (2007) Human adipose tissue-derived multipotent stem cells differentiate in vitro and in vivo into osteocyte-like cells. *Biochem Biophys Res Commun* 361:342–348.
35. Rodriguez AM, et al. (2004) Adipocyte differentiation of multipotent cells established from human adipose tissue. *Biochem Biophys Res Commun* 315:255–263.
36. Garcia T, et al. (2002) Behavior of osteoblast, adipocyte, and myoblast markers in genome-wide expression analysis of mouse calvaria primary osteoblasts in vitro. *Bone* 31:205–211.
37. Lo CM, Ferrier J (1998) Impedance analysis of fibroblastic cell layers measured by electric cell-substrate impedance sensing. *Phys Rev E Stat Phys Plasmas Fluids Relat Interdiscip Topics* 57:6982–6987.
38. Hatakeyama N, et al. (2008) IGF-I regulates tight-junction protein claudin-1 during differentiation of osteoblast-like MC3T3-E1 cells via a MAP-kinase pathway. *Cell Tissue Res* 334:243–254.
39. Wegener J, Sieber M, Galla HJ (1996) Impedance analysis of epithelial and endothelial cell monolayers cultured on gold surfaces. *J Biochem Biophys Methods* 32:151–170.
40. Urdapilleta E, Bellotti M, Bonetto FJ (2006) Impedance analysis of cultured cells: A mean-field electrical response model for electric cell-substrate impedance sensing technique. *Phys Rev E Stat Nonlin Soft Matter Phys* 74:041908.
41. Asami K, Takahashi Y, Takashima S (1989) Dielectric properties of mouse lymphocytes and erythrocytes. *Biochim Biophys Acta* 1010:49–55.
42. Maskow T, Röllich A, Fetzer I, Ackermann JU, Harms H (2008) On-line monitoring of lipid storage in yeasts using impedance spectroscopy. *J Biotechnol* 135:64–70.